

Portal Motor Velocity and Internal Force Resisting Viral DNA Packaging in Bacteriophage ϕ 29

John Peter Rickgauer,* Derek N. Fuller,* Shelley Grimes,[†] Paul J. Jardine,[†] Dwight L. Anderson,^{†‡} and Douglas E. Smith*

*Department of Physics, University of California, San Diego, La Jolla, California; and [†]Department of Diagnostic and Biological Sciences, and [‡]Department of Microbiology, University of Minnesota, Minneapolis, Minnesota

ABSTRACT During the assembly of many viruses, a powerful molecular motor compacts the genome into a preassembled capsid. Here, we present measurements of viral DNA packaging in bacteriophage ϕ 29 using an improved optical tweezers method that allows DNA translocation to be measured from initiation to completion. This method allowed us to study the previously uncharacterized early stages of packaging and facilitated more accurate measurement of the length of DNA packaged. We measured the motor velocity versus load at near-zero filling and developed a ramped DNA stretching technique that allowed us to measure the velocity versus capsid filling at near-zero load. These measurements reveal that the motor can generate significantly higher velocities and forces than detected previously. Toward the end of packaging, the internal force resisting DNA confinement rises steeply, consistent with the trend predicted by many theoretical models. However, the force rises to a higher magnitude, particularly during the early stages of packaging, than predicted by models that assume coaxial inverse spooling of the DNA. This finding suggests that the DNA is not arranged in that conformation during the early stages of packaging and indicates that internal force is available to drive complete genome ejection in vitro. The maximum force exceeds 100 pN, which is about one-half that predicted to rupture the capsid shell.

INTRODUCTION

Viruses usually are comprised of a nucleic acid chromosome packed inside a protein shell. In many double-stranded DNA (dsDNA) viruses, including the dsDNA bacteriophages and animal viruses such as adenoviruses and herpesviruses, the protein shell (prohead) is assembled before the packaging of DNA. A motor complex that derives energy from ATP pumps the DNA into the prohead (1). The bacterial virus ϕ 29 is an excellent model system for studying this process because of its highly efficient in vitro DNA packaging activity and the development of a single-molecule packaging assay (2,3).

The ϕ 29 DNA packaging motor is a stacked ring structure assembled at a unique fivefold vertex of the prolate icosahedral prohead. Embedded in this vertex is a dodecameric ring of gene product 10 (gp10) that forms the head-tail connector, which has a central channel through which the DNA is driven during packaging (4,5). Attached to the narrow end of the connector (4) is an oligomer of a viral-encoded prohead RNA (pRNA) (6–8). Binding of multiple copies of the packaging ATPase, gp16, to the pRNA ring completes the motor (4,9,10). The stoichiometry of the pRNA oligomer has been reported as either 5 (4,11) or 6 (7,8,12,13), and it is believed that gp16 has the same copy number as the pRNA, likely acting as a complex of heterodimers (2).

Previously, we developed a method for measuring the packaging of single DNA molecules in ϕ 29 using optical tweezers (3). The motor was shown to generate high forces needed to package the viral genome against increasing internal forces. These forces arise due to the tight confinement of the DNA, which experiences electrostatic self-repulsion, bending rigidity, and entropy loss (14). We suggested that the internal force that builds during packaging, estimated as high as ~ 50 pN, could at least partly drive DNA ejection during viral infection of cells.

Subsequently, there has been considerable effort put into theoretical modeling of viral DNA packaging (15–24). Building on earlier work by Riemer and Bloomfield (14) and Odijk (25), Kindt et al. and Tzllil et al. used Brownian dynamics simulations and analytical theory to predict the forces involved in DNA compaction (15,17). Their calculations, which assumed a spherical capsid, suggested that the DNA molecule would transition through toroidal and spool-like geometries with increasing length packaged, resulting in loading forces rising to tens of picoNewtons, which is of the same order of magnitude as those measured in single-molecule assays of DNA packaging of ϕ 29. In a separate study, Purohit et al. employed elasticity theory and empirically informed models for charge and hydration forces to model ϕ 29 DNA packaging, assuming an inverse-spool conformation for the DNA (16,21). They obtained results in accord with trends observed in experiments and previous calculations. They also employed continuum mechanics to estimate stresses in the capsid walls and map these to atomic forces, rationalizing how capsids withstand the measured forces without rupturing, though not by a wide margin. Most recently, Petrov and

Submitted January 23, 2007, and accepted for publication August 17, 2007.

Address reprint requests to Douglas E. Smith, Dept. of Physics, University of California, San Diego, Mail Code 0379, 9500 Gilman Dr., La Jolla, CA 92093. E-mail: des@physics.ucsd.edu.

Editor: Edward H. Egelman.

© 2008 by the Biophysical Society
0006-3495/08/01/159/09 \$2.00

doi: 10.1529/biophysj.107.104612

Harvey also modeled $\phi 29$ packaging via molecular dynamics simulation (24). They predict similar internal forces, but find variable individual DNA conformations resembling folded toroids, and a nonnegligible entropic contribution to the free-energy change.

Methods for studying phage DNA ejection have also been developed (26–29). Evilevich et al. showed that ejection with phage λ , as triggered by purified lamB receptor protein, could be inhibited by applying osmotic pressure outside the capsid with polyethylene glycol (26). When combined with theoretical calculations, these measurements permitted determination of the internal pressure and ejection forces. Internal force was found to be ~ 20 pN at the beginning of ejection in conditions similar to those used in $\phi 29$ packaging studies (buffers containing moderate concentrations of Mg^{2+} , but lacking DNA condensing agents such as polyamines) (27). Notably, it was also found that the entire λ genome could be ejected, thus indicating that there is nonnegligible internal pressure even at low capsid fillings (27,29). Specifically, a force of several pN was detected in phage λ DNA ejection experiments with one-quarter of the genome still inside the capsid (27,29). In our previous single-molecule measurements on $\phi 29$ DNA packaging, the early stages of translocation were not measured, but the internal force appeared to extrapolate to zero with one-third to one-half of the genome packaged (3). This qualitative discrepancy between these two studies is resolved in the present work.

In our previous work on $\phi 29$, we used partially packaged complexes that were stalled and then restarted during the optical tweezers measurement, and therefore could not characterize the early stages of DNA translocation (3). Here, we present an approach that allows us to measure these earlier events, and we also introduce several other improvements to our assay. We recently discovered that during packaging in the optical tweezers of the native $\phi 29$ DNA, which has terminal proteins (gp3), the initial tether length is highly variable (see Supplementary Material), most likely due to gp3-mediated looping of the DNA (30). In this work, we assembled DNA packaging complexes using a new procedure, and used a DNA construct without gp3. This method ensures reproducible initial tether lengths, allowing highly accurate determination of the length of DNA packaged throughout the packaging process. We also used a dual optical tweezers system, which further increases the accuracy of tether length measurements and increases experimental throughput (31). Finally, we also introduce a technique for measuring the packaging rate at near-zero load, where the motor is less perturbed by the act of measurement. These improvements reveal that the maximum rate of DNA translocation is $\sim 65\%$ higher and the maximum internal force resisting DNA compaction is approximately twice that detected previously. These measurements give us further insight into the function of the molecular motor and the nature of the forces resisting DNA confinement in the viral capsid.

METHODS

Sample preparation

Bacteriophage $\phi 29$ components including proheads and gp16 were purified as described previously (30). A 25,340-basepair (bp) dsDNA construct labeled at one end with biotin was prepared by polymerase chain reaction from *E. coli* DNA, as described in detail previously (31). A mixture of 2 μ g of proheads and 0.25 μ g of gp16 was made in 10 μ l of $0.5\times$ TMS buffer (25 mM Tris-HCl buffer (pH 7.8), 50 mM NaCl, and 5 mM $MgCl_2$) and incubated for 2 min. γ S-ATP (Roche Applied Science, Penzberg, Germany) was then added to a final concentration of 0.4 mM, and the sample was incubated for 45 min at room temperature. After incubation, 1 μ l of an RNase inhibitor (SUPERase-IN, Ambion) was added to the complexes.

Streptavidin-coated microspheres (2.1 μ m diameter, 5% w/v, SpheroTech, Lake Forest, IL) and protein G-coated microspheres (2.1 μ m diameter, 5% w/v, SpheroTech) were washed in phosphate-buffered saline. DNA was tethered to the streptavidin microspheres, and antiphage antibodies were attached to the protein G microspheres, as described previously (3,31). Of these microspheres, 2 μ l were added to 4.5 μ l of the prohead complexes and incubated for 45 min. Optical tweezers measurements were carried out in a three-chamber flow cell. Packaging was measured in the central chamber, whereas the two side chambers each contained one of the two types of microspheres. The two types of microspheres were then injected through two different capillary tubes into the central chamber. Only the central chamber contained ATP. Measurements were carried out in $0.5\times$ TMS supplemented with 0.5 mM ATP (the standard $\phi 29$ packaging buffer). The γ S-ATP added earlier was completely washed away when the microspheres were diluted 100-fold in $0.5\times$ TMS and then injected into the measurement chamber, causing complete buffer exchange, as described previously (3).

Optical tweezers

A dual optical trap system was used. In brief, the apparatus consists of a diode-pumped solid-state Nd:YAG laser (CrystaLaser) split into two orthogonally polarized beams that were focused by a water-immersion microscope objective (Plan Apochromat, 1.2 NA, Olympus, Melville, NY) to form two optical traps. One beam was steered by use of an acousto-optic deflector (IntraAction, Bellwood, IL) and the other was fixed. The exiting beams were collected by an identical objective, and the deflections of the fixed beam were measured at 1 kHz by imaging the back focal plane of the objective onto a position-sensing detector (On-Trak). The signal was digitized by a calibrated 16-bit data acquisition card (6035E, National Instruments, Austin, TX) that measured time with an accuracy of <1 ms. The instrument was calibrated as described previously (32), such that the DNA length was measured with an error of $<0.3\%$. The series compliance of the two optical traps was 12.3 nm/pN. Measurements were done at $\sim 23^\circ\text{C}$.

Force-extension measurements

The force versus DNA extension (end-to-end distance) was measured in the standard $\phi 29$ packaging buffer by tethering the 25.3-kbp DNA construct, labeled at one end by biotin and at the other end by digoxigenin, between a streptavidin-coated microsphere and an anti-digoxigenin-coated microsphere, as described previously (31). The measurements were made slowly enough to allow for relaxation of the trapped microspheres and the DNA. Specifically, the relaxation time of the trapped microsphere is <2 ms (based on the measured corner frequency of the Brownian fluctuations (32)) and the relaxation time of the DNA is <10 ms (33). The DNA extension was increased in small steps of 10 nm (0.12% change in fractional extension per step) at 50 Hz, such that there was sufficient time for relaxation.

Ramped DNA stretching

After detecting a DNA tether, the extension was quickly relaxed by decreasing the separation between the traps in 1- μ m steps at 50 Hz until the

fractional extension of the DNA was $<65\%$, typically reaching $\sim 30\text{--}50\%$ (tension <0.15 pN). The molecule was then stretched by increasing the separation in 8.5-nm steps ($<0.4\%$ change in fractional extension per step) at 50 Hz until the force (averaged over 60 ms) exceeded 5 pN. The molecule was then relaxed again, and this stretch-relax cycle was repeated until packaging was complete or the tether broke. There was no evidence that the 5-pN applied force caused any slipping of DNA out of the phage head during these measurements, since this would have shown up as a drop in the recorded force signal. Previously, we showed that slipping occurs very rarely with a 5-pN applied load (3). Each stretch to 5–6 pN (which corresponds to a fractional DNA extension of $\sim 95\%$) yields an accurate measurement of the DNA tether length (corresponding to a certain filling level) at that time point. The DNA length was calculated knowing the separation between the traps, force, and compliances of the traps, using the measured force versus fractional extension relationship. The length of DNA packaged is equal to the total DNA length minus the length unpackaged (the tether length) and the percent packaged is equal to the length packaged divided by the $\phi 29$ genome length. This gives us a group of discrete lengths and times from which to calculate time-averaged velocities during each stretch cycle. We calculate the changes in length and in time between all adjacent stretch events, yielding a velocity for each. The plot of velocity versus filling averaged over all datasets was obtained by binning the individual velocities from all the packaging events in 5% filling bins.

Force-clamp measurements

After a DNA molecule was tethered, the traps were quickly separated (at $10\ \mu\text{m/s}$) until the tension rose above a force set point, and feedback was then invoked to hold the force fixed at the set point. The force (averaged over 20 ms) was monitored at 50 Hz, and if it was greater or less than the force set point, the traps were moved closer or farther, respectively, by 4 nm ($<0.2\%$ change in fractional extension per step). This simple feedback method was more than sufficient for our determination of the average velocity over a 1-s or longer time interval. The DNA length was calculated knowing the separation between the traps, force, and compliances of the traps, using the measured force versus fractional extension relationship. To obtain the average velocity for each complex, the length versus time data corresponding to capsid fillings up to 10% was fit to a line by the least-squares method to obtain the slope. Large, clearly discernible pauses (velocity < 10 bp/s for > 2 s), which would skew the velocity measured with a given complex at a particular filling level sharply from the mean velocity, were removed before analysis. The ensemble average velocity was calculated by averaging these individual velocities for all packaging events measured at each particular force. This method was used to determine the motor velocity with loads up to 40 pN.

Fixed trap separation measurements

Measurements of motor velocity for total loads >40 pN were made with capsid fillings ranging from 70 to 80%, such that internal forces contributed to the total load acting on the motor. These measurements were made by holding the separation between the traps fixed, and allowing the externally applied load (DNA tension) to build as the DNA tether shortened. Only datasets in which the external force covered the range from at least 5 to 25 pN were used. The tether length was calculated knowing the separation between the traps, force, and compliances of the traps, using the measured force versus fractional extension relationship. Large, clearly discernible pauses (velocity < 10 bp/s for > 2 s), which would skew the velocity measured with a given complex at a particular force sharply from the mean velocity, were removed before analysis. Velocities were calculated by fitting the length versus time data in a 1-s window moved in 0.2-s steps (corresponding to certain average loads) to a line by the least-squares method to obtain the slope. To obtain the average velocity versus force, all of these individual velocities, from all datasets, were averaged together in 5-pN force bins.

The total load equals externally applied load (which is measured) plus internal load. The internal load was deduced from the known capsid fillings in the fixed trap measurements by relating the velocity measured in the velocity versus filling data to the velocity measured in the velocity versus total load data. The velocity versus filling data was measured with near-zero external load using the ramped DNA stretching technique and the velocity versus total load data was measured with near-zero internal load using the force-clamp method, as described above. Each measured filling value (ranging from 70 to 80%) was translated into a corresponding velocity, V , by linear interpolation of the velocity versus filling data. Each velocity V was then translated into an effective load (the deduced internal load) using the velocity versus total load data. This translation was done by fitting the velocity versus total load data (see Fig. 4 A), to the theoretical expression in Chemla et al. (34), which yields a formula for calculating total load from velocity. Errors in this calculation were estimated using 95% confidence intervals in the fit using the curve-fitting toolbox in Matlab 7 (Mathworks, Natick, MA).

RESULTS

Measurement technique

The experimental setup is shown in Fig. 1. A dual-trap optical tweezers was used to manipulate two types of microspheres. Prohead gp16 motor complexes were prepared in bulk and attached to antibody-coated microspheres before introduction into the microfluidic chamber and trapping in one of the optical traps. Similarly, DNA substrate molecules were attached to streptavidin-coated microspheres via a biotin tag, and the bead was captured in the second trap. Details are given in the Methods section. In the presence of ATP, the microspheres were brought into near contact for 1 s and then

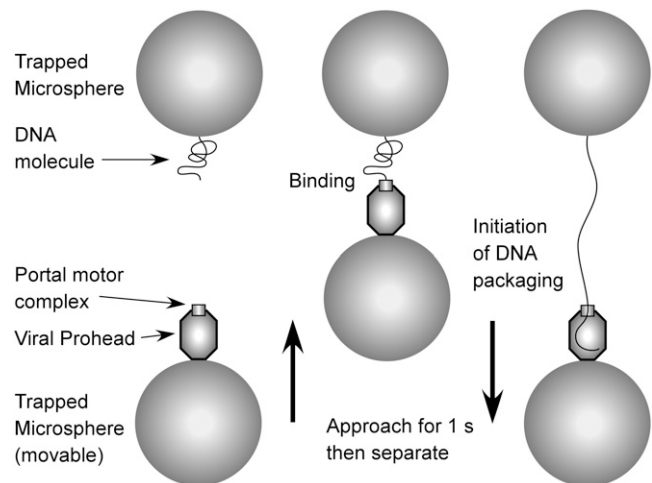


FIGURE 1 Schematic illustration of the experimental method. Microspheres carrying prohead-ATPase complexes were captured in one optical trap (*lower left sphere*) and microspheres carrying DNA molecules were captured in a second trap (*upper left sphere*). To initiate DNA packaging, the microspheres were brought into near contact for ~ 1 s (*middle*) and then separated to probe for DNA binding and translocation (*right*). The force acting on the DNA was recorded by measuring the deflection of the laser beam forming the top trap and the bottom trap was translated under computer control by use of an acousto-optic deflector.

separated to detect DNA tether formation and the nearly simultaneous initiation of translocation. By initiating DNA packaging in the optical tweezers chamber, we are able to measure the rate and force of DNA translocation over the entire length of the packaged DNA substrate, in contrast with our previous work that was only able to report on the final two-thirds of this process.

Previously, we measured the average rate of packaging versus length of DNA packaged (filling level) with an applied 5-pN external load (3). However, when viruses assemble *in vivo* there is presumably minimal external load on the DNA. The frictional drag forces have been estimated to be very small (21). Even accounting for the bacterial cytoplasm being ~ 10 -fold more viscous than water (35), the frictional drag during packaging is estimated to be $< 2 \times 10^{-3}$ pN. We therefore sought to develop a technique for measuring DNA packaging at near-zero applied load. We accomplished this by holding the DNA slack most of the time during packaging (< 0.15 pN of tension) using a ramped DNA stretching technique where we extended the DNA briefly to 5 pN at time intervals to measure the change in tether length (Fig. 2). Details are given in the Methods section.

Early DNA packaging dynamics

The improvements described above allow us to measure the motor velocity from the earliest stages of packaging to completion under near-zero external load (Fig. 3). Strikingly, we find that the DNA translocation rate decreases significantly during the first half of head-filling, rather than being constant. In addition, the average DNA translocation rate at the beginning of packaging is ~ 165 bp/s, $\sim 50\%$ higher than the

average rate of ~ 100 bp/s measured earlier with a 5-pN force clamp and the capsid partly filled (3). This difference is largely accounted for by two factors: the velocity is $\sim 25\%$ higher at near-zero filling than at one-third filling and $\sim 15\%$ higher at near-zero load than at 5 pN. The residual $\sim 10\%$ difference is attributable to the more accurate determination of the filling level provided by the new initiation method and dual optical tweezers instrument used in this study.

Velocity-load relationship of the motor

Since there is a significant decrease in velocity with filling during the earliest stages of packaging, we reevaluated the velocity versus load relationship of the motor (3,34). Previously, it was measured with at least one-third of the genome length packaged, where the motor velocity is lower. These earlier measurements were also made by holding the trap positions fixed and allowing the DNA tension to increase with ongoing packaging. Although this is a convenient method for obtaining translocation data across a range of forces in a single measurement, the capsid filling increases by ~ 10 – 15% from its initial value during such a measurement due to the compliance of the traps and DNA. This change in filling results in an increasing internal force (the force resisting DNA packaging) during the measurement that is difficult to account for. Therefore, to determine the velocity versus load more accurately in this work, we made velocity measurements at specific loads at low capsid filling (in the range 5–10%) by using feedback to control the separation between the traps, so as to maintain a constant load. These measurements were repeated with many different complexes at each load. The tether length versus time, and hence the motor velocity, was then determined at each specific force value

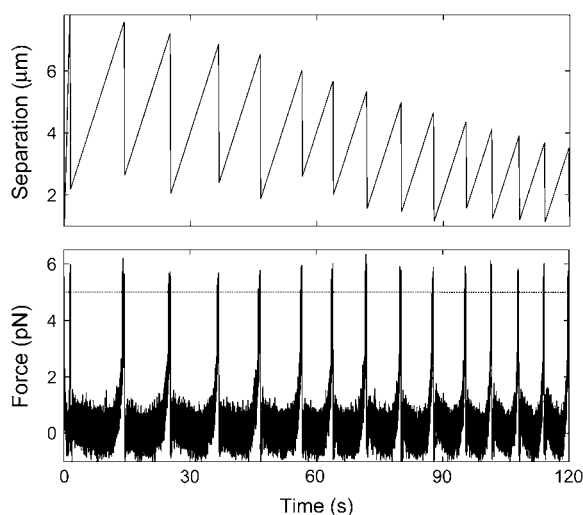


FIGURE 2 Measurement of motor velocity at near-zero load. The DNA was held slack most of the time ($F < 0.15$ pN) and periodically stretched by separating the traps until the force reached 5–6 pN (lower graph) to accurately determine the trap separation (upper graph) and, from this, the DNA tether length.

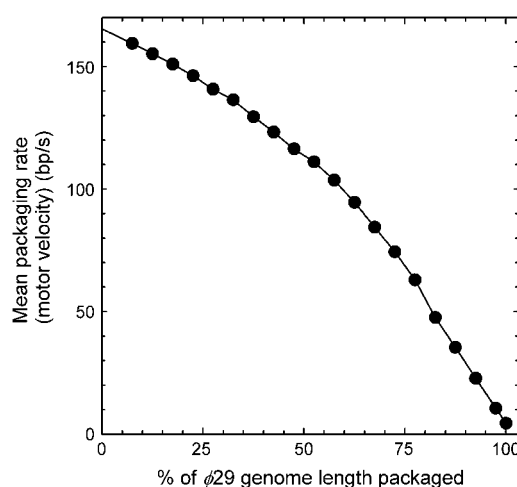


FIGURE 3 Rate of packaging versus capsid filling. Data was recorded at near-zero load using the ramped stretching method (average over $N = 24$ complexes). Standard errors on the measurements are approximately equal to the size of the solid circles (~ 3 bp/s).

(Fig. 4). This method was used for loads up to 40 pN. Details are given in the Methods section.

When the externally applied force exceeded ~ 40 pN, rapid breakage of DNA tethers (likely due to failure of the prohead-antibody linkage) made data collection difficult. Therefore, to determine the motor velocity versus force for higher forces, we made measurements with capsid fillings ranging from 70 to 80%, such that an internal force contributed to the total force acting on the motor, as described in Methods. Thus, by adding an applied external load to the internal load, we access total loads >40 pN.

As shown in Figs. 3 and 4, motor velocity decreases with increasing capsid filling and also decreases with increasing

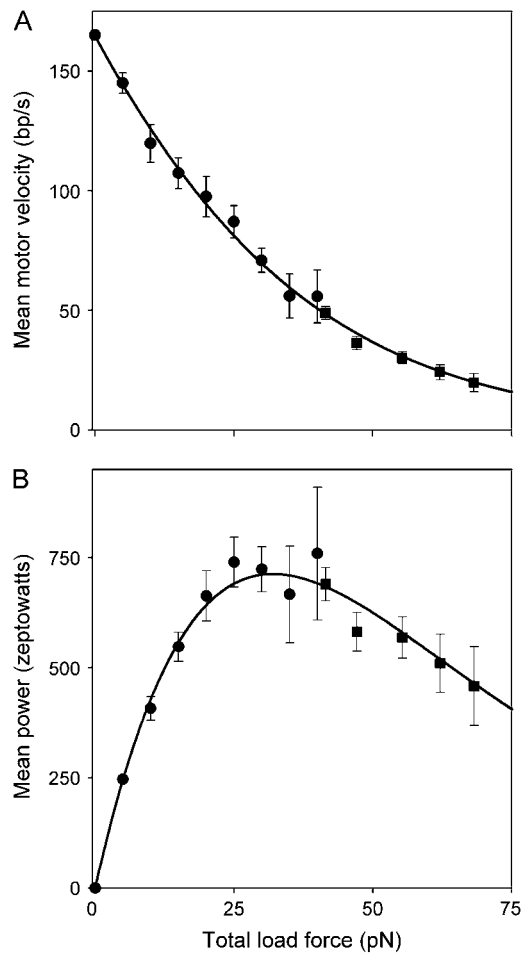


FIGURE 4 (A) Rate of packaging versus total load acting on the motor. Each velocity was determined as an average of $N = 6$ to 34 complexes (mean $N = 17$, error bars indicate standard errors). Data for total loads <40 pN (circles) were recorded at 5–10% capsid filling, where the internal force is negligible. Data for total loads >40 pN (squares) were collected at 70–80% capsid filling, where both external and internal load contributed. The contribution of internal load for loads >40 pN was determined from the known filling using the velocity versus filling data (Fig. 3) and low-force velocity versus load data, as described in the text. The solid line is a fit of the data to the theoretical expression in Chemla et al. (34). (B) Average power generated by the motor versus load. Note that 1 zeptowatt = 10^{-21} watts $\cong 3$ pN·bp/s.

load. The decrease in velocity with filling occurs due to the buildup of internal force (i.e., the force resisting DNA confinement) (3). The internal force is deduced by relating the velocity measured in the velocity versus filling data to the velocity measured in the velocity versus force data, to obtain force versus filling (Fig. 5). Details are given in Methods. Our measurements reveal a significant internal force during the early stages of packaging, rising to a value of ~ 7 pN at one-third filling ($\sim 6\%$ of the maximum) and ~ 14 pN at half filling ($\sim 12\%$ of the maximum). The slope of the force versus filling curve increases continuously, such that the internal force increases sharply during the final stages of filling. Such behavior is in accord with the trend predicted by recent theoretical models (15–18,20–22,24,36). We find that the internal force extrapolates to 110 ± 9 pN, requiring one of the highest force generations reported for a biological molecular motor. Recent theoretical calculations suggest that this internal force is only a factor of 2 lower than that needed to disrupt the protein-protein interactions that stabilize the capsid shell (16). However, recent studies in which the capsid was indented by an AFM tip found that the capsid could withstand indentation forces up to ~ 1000 pN (37), a finding that is compatible with the capsid being able to withstand the 110 pN of internal force detected in our experiments.

DISCUSSION

Impact of improved measurement techniques

The ability to obtain rate measurements from near-zero filling to head full under zero-load conditions allows us to reinterpret the nature of $\phi 29$ DNA packaging and the physics

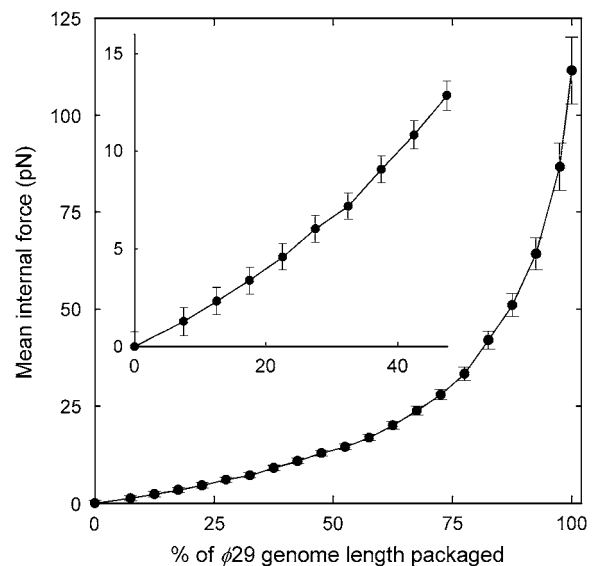


FIGURE 5 Mean internal force versus capsid filling deduced from the results in Figs. 3 (rate versus filling) and 4 A (rate versus load). The inset plot is a magnified view showing the force increase during the early stages of packaging. The error bars were calculated as described in the text.

of DNA compaction. First, rate and force have been measured during translocation of the first third of the head-full complement of DNA, revealing a decrease in packaging rate throughout the whole process of translocation rather than only the last half. Second, the higher rates of translocation measured here due to the zero-load approach reveal a more accurate picture of the response of the motor to internal load. In combination, these improvements have a significant impact on our understanding of the packaging dynamics.

Motor characteristics

The average motor velocity at high external load determined previously was underestimated due to the use of the fixed-trap measurement mode and the tendency of the motor to pause and tethers to break at high external loads. With our improved measurement technique and increased statistics we find that the average velocity approaches but does not reach zero with increasing force over the measured force range. Such asymptotic behavior at high force is consistent with the prediction of a recent theoretical model describing the mechanochemical kinetics of the $\phi 29$ motor (34). By multiplying force by velocity we may also calculate the average power generated by the motor and plot it as a function of applied load (Fig. 4 B). A maximum of ~ 700 zeptowatts (700×10^{-21} watts) is measured at 30 pN load and 65 bp/s motor velocity.

Comparisons with theory of internal forces resisting DNA confinement

The magnitude of the force detected at low filling is similar to that inferred during the latter stages of DNA ejection in the phage λ system (27,29). Thus, the forces observed to build during packaging could potentially drive complete ejection of the DNA from $\phi 29$ under in vitro conditions. We note that DNA ejection into a cell is expected to encounter additional resistance due to intracellular osmotic pressure (26) and may also be aided by the action of other DNA translocating motors (38–40).

Several theoretical models propose that the DNA is arranged as a coaxial spool with hoops of DNA arranged in a hexagonal lattice filling inward from the outermost radii (14,16,21,25). The free energy is calculated as the sum of the bending energy and an empirically determined interstrand interaction energy that accounts for electrostatic self-repulsion and hydration effects; the energy is minimized by balancing these two terms. The predictions of this model, which have been calculated for the specific case of $\phi 29$ (21), are in qualitative agreement with our experimental findings. The internal force is predicted to rise sharply at the final stages of filling to a value on the same order of magnitude as that found experimentally, suggesting that the model correctly captures the essential physics. Recent molecular dynamics simulations also yield similar predictions (24). At a quantitative

level, however, the agreement between experiment and theory is not perfect. The maximum force is predicted to be ~ 50 pN in a solution containing 50 mM Na^+ , using an interaction potential based on DNA condensation measurements and a capsid volume estimated from cryoelectron microscopy (cryo-EM) images (21). This calculated force is roughly a factor of 2 lower than the 110 pN we find in a solution containing 50 mM Na^+ and 5 mM Mg^{2+} , a condition which is expected to screen more strongly than 50 mM Na^+ alone.

The inverse spool model also predicts a lower internal force at low filling than we find experimentally. For example, it predicts < 1 pN at 25% filling with 50 mM Na^+ when using the interaction potential determined from DNA condensation data (P. K. Purohit, University of Pennsylvania, personal communication, 2006), whereas we measure 5 pN at this point. This discrepancy is not completely attributable to the assumed interaction potential parameters. If these parameters are determined by fitting the model to our data at high force (e.g., at 50 pN, which occurs at $\sim 87\%$ filling), instead of using the condensation data, the predicted force at 25% filling is still < 1 pN (P. K. Purohit, University of Pennsylvania, personal communication, 2006). This comparison indicates that the experimental curve has a slightly different shape than that predicted by the model. The predictions of the model agree with our data better at high filling than at low filling, although we detect higher force across the entire range of fillings. Below, we discuss several possible reasons for these discrepancies between experiment and theory.

Frictional dissipation

If energy dissipation occurs during packaging, the mechanical work done, which is what we measure experimentally, would be higher than the gain in potential energy of the confined DNA, and this would explain our finding a higher-than-predicted packaging force. Purohit et al. (21) have estimated that viscous dissipation forces due to displacement of water from the capsid would be negligible, but other sources of friction may be present, such as that between the DNA and motor or capsid wall and between DNA segments inside the capsid (41,42). On the other hand, observations of occasional slipping during $\phi 29$ DNA packaging (3) and of DNA ejection from bacteriophages T5 (28) and λ (43), indicate that DNA can exit the capsid at > 10 kbp/s, a rate two orders of magnitude faster than the rate of packaging. These observations suggest that there is little frictional resistance to DNA movement within the capsid, in which case frictional dissipation is unlikely to explain our findings.

Interaction potentials

The disagreement between theory and experiments may indicate that the empirical DNA-DNA intrastrand repulsion potentials derived from DNA condensation experiments (44)

are not universally applicable to describe DNA packaged in all types of phages in all solution conditions. One notable difference is that the DNA segments are highly bent inside the viral capsid, whereas straight bundles of molecules were studied in the condensation experiments (44). Interaction potentials for counterion-screened DNA segments are difficult to calculate theoretically from first principles, but continuing work on this problem (42) may help to reconcile our findings with theory.

Arrangement of the DNA

Since the inverse spool model accurately predicts the ejection force in phage λ , the observation of a higher internal force may indicate that the DNA conformation during packaging in ϕ 29 is different (and less energetically optimal) than that assumed in the theoretical model. The DNA conformation in ϕ 29, which has a prolate icosahedral capsid, may also be different than that in λ , which has a larger isometric icosahedral capsid. Recent cryo-EM 3D reconstruction of P22 and epsilon15 phages (45–47) have been interpreted as indicating some degree of spooling of the DNA around the portal axis; however, similar reconstructions of ϕ 29 do not appear to reveal such organization (48, 49). Moreover, many dynamic simulations do not observe formation of a coaxial spool (15,19,20,22–24,36,49). Thus, the measured internal force in ϕ 29 may be higher than predicted because the DNA is packed in a configuration that is more energetically costly. Factors that may influence the DNA conformation are the shape of the capsid (23), the rate of packaging (36), and the degree of DNA twisting during packaging (22).

The observed build-up of internal force during the early stages of packaging appears to be in qualitative agreement with the Brownian dynamics simulations by Kindt et al. (15). These simulations find that the DNA conformation would evolve from a disordered structure, giving rise to forces of several piconewtons at low filling, into a compressed spool-like structure at high filling. A number of other recent simulations using a wide variety of methods, including equilibrium thermodynamics calculations for a confined thick polymer (18), stochastic rotation dynamics simulations of a bead-spring model (20,23), and dynamic simulations of discrete worm-like chains (22,36) also predict disordered conformations and nonnegligible internal forces during the early stages of packaging.

In the inverse spool model, the DNA conformation is also assumed to be at equilibrium at all points in time during packaging. However, given the rapid rate of the DNA translocation, it is possible that the packed DNA does not immediately equilibrate. Studies of DNA knotting inside of phage P4 suggest there is some freedom for the DNA to rearrange after packaging (50), and recent dynamic simulations find that ejection forces can be lower than packaging forces when the packaged DNA is allowed to relax before it is ejected (23). A recent molecular dynamics simulation also

found an appreciable difference between equilibrated internal energy and work done during packaging (24). The time-scale on which any relaxation may take place in an actual phage is unknown, but it could be longer than the several-minute duration of our packaging experiments.

CONCLUSIONS

We have presented improved optical tweezers measurements of DNA packaging in bacteriophage ϕ 29 that reveal the dynamics during the early stages of capsid filling and motor response over a wider range of forces. The ramped DNA stretching technique described here should also be applicable to studies of many other molecular motors. We find that the ϕ 29 packaging motor is capable of generating higher velocities and forces than detected previously. These measurements improve our understanding of the motor function and physics of DNA confinement. The detection of appreciable internal forces at low filling suggests that the DNA does not adopt a coaxial spool conformation during the early stages of packaging and that the forces that build during packaging are available to drive complete ejection of the ϕ 29 genome in vitro. The sharp increase in internal force with filling during the latter stages of packaging is in qualitative accord with many recent theoretical calculations, but none predict forces as high as those we detect. Our results suggest that further theoretical and structural studies on the DNA conformation and nature of the DNA-DNA interaction potentials will be essential to a full understanding of DNA packaging in ϕ 29.

SUPPLEMENTARY MATERIAL

To view all of the supplemental files associated with this article, visit www.biophysj.org.

Note added in proof: Recently we have extended the optical tweezers method to study ionic effects on packaging and distinct behaviors of packaging motors in the bacteriophage λ and T4 systems (51–53).

We thank R. Millin, D. Raymer, A. Schweitzer, and M. White for assistance, and P. Grayson, R. Phillips, and P. Purohit for discussions and for communicating unpublished results.

Our research was supported by the National Institutes of Health (grants GM-071552 and DE-03606), The Burroughs-Wellcome Fund, The Kinship Foundation, and the Arnold and Mabel Beckman Foundation.

REFERENCES

1. Jardine, P. J., and D. Anderson. 2006. DNA packaging in double-stranded DNA bacteriophages. In *The Bacteriophages*. R. Calendar, editor. Oxford University Press, Oxford, UK.
2. Grimes, S., P. J. Jardine, and D. Anderson. 2002. Bacteriophage ϕ 29 DNA packaging. *Adv. Virus Res.* 58:255–294.
3. Smith, D. E., S. J. Tans, S. B. Smith, S. Grimes, D. L. Anderson, and C. Bustamante. 2001. The bacteriophage ϕ 29 portal motor can package DNA against a large internal force. *Nature*. 413:748–752.

4. Simpson, A. A., Y. Tao, P. G. Leiman, M. O. Badasso, Y. He, P. J. Jardine, N. H. Olson, M. C. Morais, S. Grimes, D. L. Anderson, T. S. Baker, and M. G. Rossmann. 2000. Structure of the bacteriophage ϕ 29 DNA packaging motor. *Nature*. 408:745–750.
5. Guasch, A., J. Pous, B. Ibarra, F. X. Gomis-Ruth, J. M. Valpuesta, N. Sousa, J. L. Carrascosa, and M. Coll. 2002. Detailed architecture of a DNA translocating machine: the high-resolution structure of the bacteriophage ϕ 29 connector particle. *J. Mol. Biol.* 315:663–676.
6. Guo, P. X., S. Erickson, and D. Anderson. 1987. A small viral RNA is required for in vitro packaging of bacteriophage ϕ 29 DNA. *Science*. 236:690–694.
7. Zhang, F., S. Lemieux, X. Wu, D. St-Arnaud, C. T. McMurray, F. Major, and D. Anderson. 1998. Function of hexameric RNA in packaging of bacteriophage ϕ 29 DNA in vitro. *Mol. Cell*. 2:141–147.
8. Guo, P., C. Zhang, C. Chen, K. Garver, and M. Trottier. 1998. Inter-RNA interaction of phage ϕ 29 pRNA to form a hexameric complex for viral DNA transportation. *Mol. Cell*. 2:149–155.
9. Shu, D., and P. Guo. 2003. Only one pRNA hexamer but multiple copies of the DNA-packaging protein gp16 are needed for the motor to package bacterial virus ϕ 29 genomic DNA. *Virology*. 309:108–113.
10. Lee, T. J., and P. Guo. 2006. Interaction of gp16 with pRNA and DNA for genome packaging by the motor of bacterial virus ϕ 29. *J. Mol. Biol.* 356:589–599.
11. Morais, M. C., Y. Tao, N. H. Olson, S. Grimes, P. J. Jardine, D. L. Anderson, T. S. Baker, and M. G. Rossmann. 2001. Cryoelectron-microscopy image reconstruction of symmetry mismatches in bacteriophage ϕ 29. *J. Struct. Biol.* 135:38–46.
12. Ibarra, B., J. R. Castón, O. Llorca, M. Valle, J. M. Valpuesta, and J. L. Carrascosa. 2000. Topology of the components of the DNA packaging machinery in the phage 29 prohead. *J. Mol. Biol.* 298:807–815.
13. Shu, D., H. Zhang, J. Jin, and P. Guo. 2007. Counting of six pRNAs of phi29 DNA-packaging motor with customized single-molecule dual-view system. *EMBO J.* 26:527–537.
14. Riemer, S. C., and V. A. Bloomfield. 1978. Packaging of DNA in bacteriophage heads: some considerations on energetics. *Biopolymers*. 17:785–794.
15. Kindt, J., S. Tzllil, A. Ben-Shaul, and W. M. Gelbart. 2001. DNA packaging and ejection forces in bacteriophage. *Proc. Natl. Acad. Sci. USA*. 98:13671–13674.
16. Purohit, P. K., J. Kondev, and R. Phillips. 2003. Mechanics of DNA packaging in viruses. *Proc. Natl. Acad. Sci. USA*. 100:3173–3178.
17. Tzllil, S., J. T. Kindt, W. M. Gelbart, and A. Ben-Shaul. 2003. Forces and pressures in DNA packaging and release from viral capsids. *Biophys. J.* 84:1616–1627.
18. Marenduzzo, D., and C. Micheletti. 2003. Thermodynamics of DNA packaging inside a viral capsid: the role of DNA intrinsic thickness. *J. Mol. Biol.* 330:485–492.
19. LaMarque, J. C., T. Le, and S. C. Harvey. 2004. Packaging double-helical DNA into viral capsids. *Biopolymers*. 73:348–355.
20. Ali, I., D. Marenduzzo, and J. M. Yeomans. 2004. Dynamics of polymer packaging. *J. Chem. Phys.* 121:8635–8641.
21. Purohit, P. K., M. M. Inamdar, P. D. Grayson, T. M. Squires, J. Kondev, and R. Phillips. 2005. Forces during bacteriophage DNA packaging and ejection. *Biophys. J.* 88:851–866.
22. Spakowitz, A. J., and Z. G. Wang. 2005. DNA packaging in bacteriophage: is twist important? *Biophys. J.* 88:3912–3923.
23. Ali, I., D. Marenduzzo, and J. M. Yeomans. 2006. Polymer packaging and ejection in viral capsids: shape matters. *Phys. Rev. Lett.* 96:208102.
24. Petrov, A. S., and S. C. Harvey. 2007. Structural and thermodynamic principles of viral packaging. *Structure*. 15:21–27.
25. Odijk, T. 1998. Hexagonally packed DNA within bacteriophage T7 stabilized by curvature stress. *Biophys. J.* 75:1223–1227.
26. Evilevitch, A., L. Lavelle, C. M. Knobler, E. Raspaud, and W. M. Gelbart. 2003. Osmotic pressure inhibition of DNA ejection from phage. *Proc. Natl. Acad. Sci. USA*. 100:9292–9295.
27. Evilevitch, A., M. Castelnovo, C. M. Knobler, and W. M. Gelbart. 2004. Measuring the force ejecting DNA from phage. *J. Phys. Chem. B*. 108:6838–6843.
28. Mangenot, S., M. Hochrein, J. Radler, and L. Letellier. 2005. Real-time imaging of DNA ejection from single phage particles. *Curr. Biol.* 15:430–435.
29. Grayson, P., A. Evilevitch, M. M. Inamdar, P. K. Purohit, W. M. Gelbart, C. M. Knobler, and R. Phillips. 2006. The effect of genome length on ejection forces in bacteriophage λ . *Virology*. 348:430–436.
30. Grimes, S., and D. Anderson. 1997. The bacteriophage ϕ 29 packaging proteins supercoil the DNA ends. *J. Mol. Biol.* 266:901–914.
31. Fuller, D. N., G. J. Gemmen, J. P. Rickgauer, A. Dupont, R. Millin, P. Recouvreur, and D. E. Smith. 2006. A general method for manipulating DNA sequences from any organism with optical tweezers. *Nucleic Acids Res.* 34:e15.
32. Rickgauer, J. P., D. N. Fuller, and D. E. Smith. 2006. DNA as a metrology standard for length and force measurements with optical tweezers. *Biophys. J.* 91:4253–4257.
33. Meiners, J. C., and S. R. Quake. 2000. Femtonewton force spectroscopy of single extended DNA molecules. *Phys. Rev. Lett.* 84:5014–5017.
34. Chemla, Y. R., K. Aathavan, J. Michaelis, S. Grimes, P. J. Jardine, D. L. Anderson, and C. Bustamante. 2005. Mechanism of force generation of a viral DNA packaging motor. *Cell*. 122:683–692.
35. Elowitz, M. B., M. G. Surette, P. E. Wolf, J. B. Stock, and S. Leibler. 1999. Protein mobility in the cytoplasm of *Escherichia coli*. *J. Bacteriol.* 181:197–203.
36. Forrey, C., and M. Muthukumar. 2006. Langevin dynamics simulations of genome packing in bacteriophage. *Biophys. J.* 91:25–41.
37. Ivanovska, I. L., P. J. de Pablo, B. Ibarra, G. Sgalari, F. C. MacKintosh, J. L. Carrascosa, C. F. Schmidt, and G. J. L. Wuite. 2004. Bacteriophage capsids: tough nanoshells with complex elastic properties. *Proc. Natl. Acad. Sci. USA*. 101:7600–7605.
38. Zavriev, S. K., and M. F. Shemyakin. 1982. RNA polymerase-dependent mechanism for the stepwise T7 phage DNA transport from the virion into *E. coli*. *Nucleic Acids Res.* 10:1635–1652.
39. Kemp, P., M. Gupta, and I. J. Molineux. 2004. Bacteriophage T7 DNA ejection into cells is initiated by an enzyme-like mechanism. *Mol. Microbiol.* 53:1251–1265.
40. Gonzales-Huici, V., M. Salas, and J. M. Hermoso. 2004. The push-pull mechanism of bacteriophage ϕ 29 DNA injection. *Mol. Microbiol.* 52:529–540.
41. Gabashvili, I. S., and A. Grosberg. 1992. Dynamics of double stranded DNA reptation from bacteriophage. *J. Biomol. Struct. Dyn.* 9:911–920.
42. Odijk, T. 2004. Statics and dynamics of condensed DNA within phages and globules. *Philos Transact. A Math. Phys. Eng. Sci.* 362:1497–1517.
43. Grayson, P., L. Han, T. Winther, and R. Phillips. 2007. Real-time observations of single bacteriophage λ DNA ejections in vitro. *Proc. Natl. Acad. Sci. USA*. 104:14652–14657.
44. Strey, H. H., R. Podgornik, D. C. Rau, and V. A. Parsegian. 1998. DNA-DNA interactions. *Curr. Opin. Struct. Biol.* 8:309–313.
45. Lander, G. C., L. Tang, S. R. Casjens, E. B. Gilcrease, P. Prevelige, A. Poliakov, C. S. Potter, B. Carragher, and J. E. Johnson. 2006. The structure of an infectious P22 virion shows the signal for headful DNA packaging. *Science*. 312:1791–1795.
46. Chang, J., P. Weigele, J. King, W. Chiu, and W. Jiang. 2006. Cryo-EM Asymmetric reconstruction of bacteriophage P22 reveals organization of its DNA packaging and infecting machinery. *Structure*. 14:1073–1082.
47. Jiang, W., J. Chang, J. Jakana, P. Weigele, J. King, and W. Chiu. 2006. Structure of ϕ 15 bacteriophage reveals genome organization and DNA packaging/injection apparatus. *Nature*. 439:612–616.
48. Xiang, Y., M. Morais, A. Battisti, S. Grimes, P. Jardine, D. Anderson, and M. Rossmann. 2006. Structural changes of bacteriophage ϕ 29 upon DNA packaging and release. *EMBO J.* 25:5229–5239.
49. Comolli, L. R., A. J. Spakowitz, C. E. Siegerist, P. J. Jardine, S. Grimes, D. L. Anderson, C. Bustamante, and K. H. Downing. 2007. Three-dimensional architecture of the bacteriophage ϕ 29 packaged

- genome and elucidation of its packaging process. *Virology*. In press. doi:10.1016/j.virol.2007.07.035.
50. Arsuaga, J., M. Vazquez, P. McGuirk, S. Trigueros, D. Summers, and J. Roca. 2005. DNA knots reveal a chiral organization of DNA in phage capsids. *Proc. Natl. Acad. Sci. USA*. 102:9165–9169.
51. Fuller, D. N., J. P. Rickgauer, P. J. Jardine, S. Grimes, D. L. Anderson, and D. E. Smith. 2007. Ionic effects on viral DNA packaging and portal motor function in bacteriophage ϕ 29. *Proc. Nat. Acad. Sci. USA*. 104:11245–11250.
52. Fuller, D. N., D. M. Raymer, J. P. Rickgauer, R. M. Robertson, C. E. Catalano, D. L. Anderson, S. Grimes, and D. E. Smith. 2007. Measurements of single DNA molecule packaging dynamics in bacteriophage λ reveal high forces, high motor processivity, and capsid transformations. *J. Mol. Biol.* 373:1113–1122.
53. Fuller, D. N., D. M. Raymer, V. I. Kottadiel, V. B. Rao, and D. E. Smith. 2007. Single phage T4 DNA packaging motors exhibit large force generation, high velocity, and dynamic variability. *Proc. Nat. Acad. Sci. USA*. 104:16868–16873.